J Clust Sci (2016) 27:285–298
DOI 10.1007/s10876-015-0929-z

ORIGINAL PAPER

Biogenic Synthesis of Silver Nanoparticles Using *Cnidium officinale* Extract and Their Catalytic Reduction of 4-Nitroaniline

Thomas Nesakumar Jebakumar Immanuel Edison[1] · Ek Raj Baral[1] · Yong Rok Lee[1] · Sung Hong Kim[2]

Received: 8 September 2015 / Published online: 15 October 2015
© Springer Science+Business Media New York 2015

Abstract Silver nanoparticles (AgNPs) with two different morphologies were synthesized using aqueous extract of *Cnidium officinale* rhizomes under different reaction conditions and applied to the facile aqueous phase reduction of 4-nitroaniline (4-NA) as catalysts. The synthesized AgNPs are characterized by UV–Visible spectroscopy, Fourier transform infrared (FT-IR) spectroscopy, X-ray diffraction (XRD) method and high resolution transmission electron microscopy (HR-TEM) with energy dispersive X-ray spectroscopy (EDS) analysis. HR-TEM showed that the synthesized AgNPs had two different morphological forms; truncated triangular prism shapes with a mean size of $\sim$35 nm and spherical shapes with a mean size of $\sim$9 nm. The HR-TEM and XRD results are consistent with the standard values. The catalytic activities of both AgNPs were compared on the reduction of 4-NA in water by $NaBH_4$ as a reducing agent. The reduction of 4-NA was monitored using UV–Visible spectroscopy. The $\sim$9 nm (spherical) sized AgNPs showed superior catalytic activity than the larger AgNPs. The calculated rate constant (k) for the catalytic reduction of 4-nitroanilie by spherical AgNPs was 11.16×10^{-3} s^{-1}.

Keywords Silver nanoparticles · Biogenic synthesis · *Cnidium officinale* · Catalyst · 4-Nitroaniline

✉ Yong Rok Lee
yrlee@yu.ac.kr

[1] School of Chemical Engineering, Yeungnam University, Gyeongsan 712-749, Republic of Korea

[2] Analysis Research Division, Daegu Center, Korea Basic Science Institute, Daegu 702-701, Republic of Korea

Introduction

Nanotechnology involves a detailed study of materials with one or more dimensions of approximately 100 nm or less, where the properties are significantly different from those of their bulk counterparts [1–3]. The synthesis of different types of nanoparticles with different functionality and high activity has attracted considerable attention. Generally, researchers have identified four major classes of nanoparticles; metal nanoparticles, semiconductor nanoparticles, oxide nanoparticles, and polymeric nanoparticles [4]. The applications of these nanoparticles are industrially important. Among these nanoparticles, metal nanoparticles have attracted great interest for their medical, catalysis, energy, sensors, and optics applications [5–7]. Among these metal nanoparticles, silver nanoparticles (AgNPs) play a vital role because of their huge applications and low cost compared to other noble metal nanoparticles. AgNPs absorb strongly at ~400 nm owing to the surface plasmon resonance (SPR). AgNPs have been synthesized using a range of methods, such as biological reduction methods (plant extracts, fungi and fruits), chemical reduction methods, sol–gel methods, electrochemical methods, laser ablation methods, ultrasonic methods, and microwave methods [8–12]. Compared to other methods, the reduction of Ag^+ ions using plant extracts has many advantages. The main advantages are as follows: plant extracts act as reducing and capping agents; are eco-friendly, easily available, and quite comfortable for the synthesis of metal nanoparticles with different sizes and shapes; and are inexpensive [13–15].

Cnidium officinale Makino, a medicinal plant belonging to the family *Umbelliferae*, is distributed widely in South Korea and Japan. The rhizome of this plant is used as medicine for the treatment of pain, inflammation, menstrual disturbances, and antivitamin deficiency disease [16, 17]. The major phytoconstituents present in the rhizomes are falcarindiol, 6-hydroxy-7-methoxydihydroligustilide, ligustilidiol, cnidilide, ligustilide, butylphthalide, neocnidilide, and butylidenephthalide [18–20].

4-Nitroaniline (4-NA) is largely consumed industrially as a precursor in the synthesis of p-phenylenediamine. The conversion of 4-NA to p-phenylenediamine can be achieved by hydrogenation in the presence of iron metal as a catalyst [21]. 4-NA is readily soluble in water, methanol and ethanol, and is used mainly in the synthesis of dyes. The compound is quite toxic to humans and all aquatic organisms. 4-NA can cause long-term environmental damage if released as a pollutant. The reduction of 4-NA is industrially and environmentally important [22].

This paper describes the facile biosynthesis of AgNPs with two different morphologies using an aqueous extract of *Cnidium officinale* rhizomes. The catalytic ability of the synthesized AgNPs used for the reduction of 4-NA using $NaBH_4$ is also reported.

Materials and Methods

Materials

Dried *Cnidium officinale* rhizomes were received from a local market in Yeongchon, South Korea. Silver nitrate, 4-nitroaniline and Sodium borohydride were purchased from Sigma-Aldrich. The double distilled (DD) water was used throughout this study.

Methods

Preparation of Aqueous Extract

The dried *Cnidium officinale* rhizomes were cut into small pieces and ground using a mortar. Powdered rhizomes (5 g) were extracted with 100 mL of DD water in a clean conical flask at 80° C for 15 min. After extraction, the supernatant liquid was filtered through a Whatman filter paper. The clean supernatant liquid was used for the synthesis of AgNPs.

Synthesis of AgNPs

To determine the effects of concentration on the synthesis of AgNPs, two types of reactions were carried out separately. In the first reaction, 5 mL of the aqueous extract was added to 15 mL of an $AgNO_3$ solution (0.01 M) in a 25 mL vial. In the second reaction, 2 mL of the extract was mixed with 18 mL of $AgNO_3$ (0.01 M) solution. The total reaction volume was fixed to 20 mL. The effect of pH on the synthesis of AgNPs was also studied. All reactions were carried out at room temperature (25° C).

Characterization of AgNPs

The effects of the extract concentration and pH on the synthesis of AgNPs was monitored by a visual inspection and a double beam UV–Vis spectrophotometer (OPTIZEN 3220UV). For UV–Vis spectroscopy analysis, 0.5 mL of the sample was diluted by adding 2.5 mL of DD water. The absorbance was measured over the wavelength range, 200–800 nm (scan rate 2 nm/s).

The completely dried aqueous extract and dried AgNPs were pelletized separately with KBr and FT-IR analysis was carried out using a JASCO FT-IR spectrometer.

The synthesized AgNPs were drop coated onto 1 × 1 cm dimensioned clean glass plates and XRD was performed using a PANalytical X'Pert^3 MRD diffractometer. The analyses were conducted using Cu Kα radiation ($\lambda = 1.54$ Å) at 40 kV and 30 mA.

The synthesized AgNPs were cleaned completely and diluted with distilled water to achieve an absorbance intensity range of ~0.5 a.u. using a UV–Vis spectrophotometer. For high resolution transmission electron microscopy (HR-TEM), one drop of the AgNPs was placed onto a carbon coated copper disc. After drying, HR-TEM was carried out using a FEI-Tecnai TF 20 transmission electron microscope operating at an acceleration voltage of 200 kV with a point resolution of 0.24 nm and a Cs of 1.2 mm. EDS was also performed using the same instrument.

Protocol for Measuring the Catalytic Activity of AgNPs

The reduction of 4-NA was carried out in a quartz cuvette with a 1 cm path length and a 3.5 mL total volume. The catalytic activities of the two different AgNPs (2 mL extract and pH 9) were tested. To determine the optimal concentration of reactants and catalyst, several experiments were carried out, and the concentration of reactants and catalyst were fixed as stated below. The concentrations of the AgNPs were fixed by the intensity of absorbance to 0.25 a.u. In a typical reaction, 0.30 mL of 4-NA (0.01 M), 1.68 mL of DD water, 1 mL of $NaBH_4$ (0.05 M), and 0.02 mL of AgNPs were mixed. The corresponding time dependent UV–Vis response was monitored within the range from 200 to 500 nm (scan rate is 5 nm/s) using an OPTIZEN 3220UV photometer.

Results and Discussion

Characterization of AgNPs Synthesized Using *Cnidium officinale*

The colloidal AgNPs are absorbed in the visible region (~400 nm) owing to the interaction between the light energy and free electrons present in the nanopartilces, known as surface plasmon resonance (SPR) [23]. The SPR peak is quite sensitive and depends on the size, shape, agglomeration nature, and concentration of AgNPs [24]. The UV–Visible spectroscopy is a valuable tool for analyzing the SPR peak. After adding the extract, the appearance of brownish yellow color was noticed after a 24 h reaction. This indicates the formation of AgNPs [25]. The photographic images are shown in Fig. 1. The time dependent UV–Vis spectra of AgNPs

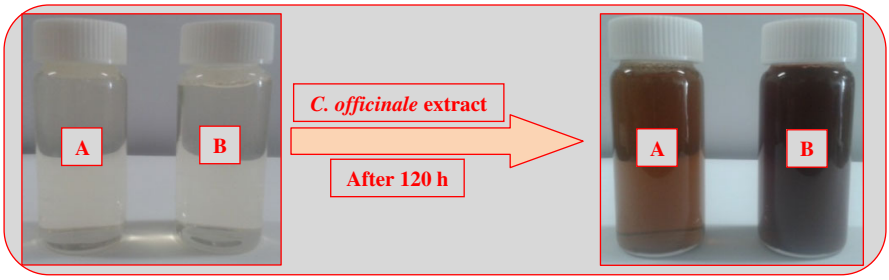

Fig. 1 Synthesis of AgNPs using A (2 mL) and B (5 mL) of *C. officinale* extract

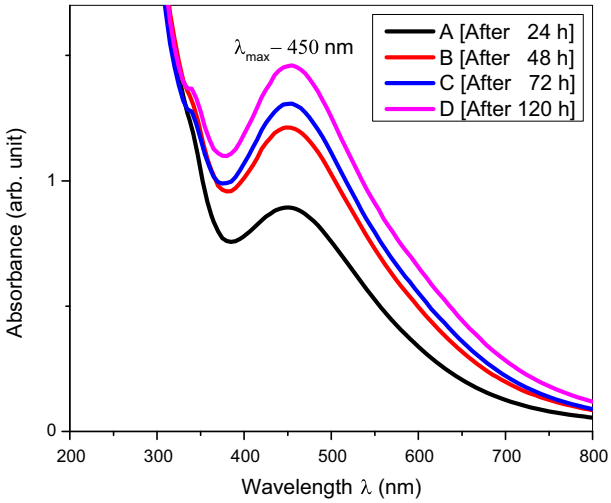

Fig. 2 UV–Vis spectra of AgNPs synthesized using 5 mL of *C. officinale* extract

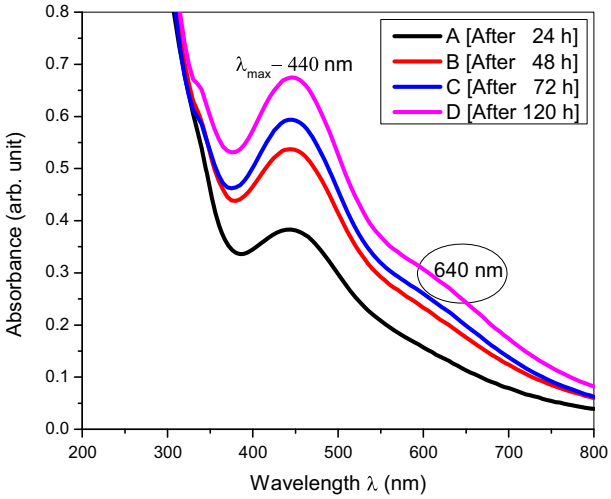

Fig. 3 UV–Vis spectra of AgNPs synthesized using 2 mL of *C. officinale* extract

synthesized using different concentration of *C. officinale* are shown in Figs. 2 and 3. From the figures, formation of AgNPs is dependent on the reaction time as well as the concentration of the extract [26]. A comparison of the absorbance intensity of the SPR peak showed that the formation of AgNPs synthesized using 5 mL of the extract was faster than in the 2 mL of the extract. The synthesized AgNPs absorbed at 450 nm (5 mL extract) and 440 nm (2 mL extract). The size of the synthesized AgNPs using 2 mL of the extract is must be smaller than that of the other one identified from λ_{max} of the SPR peak (appeared at a lower wavelength) [27].

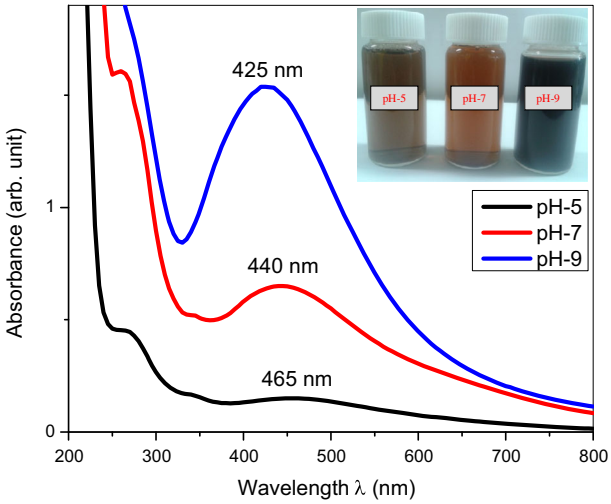

Fig. 4 Effect of pH on the synthesis of AgNPs using 2 mL of *C. officinale* extract at 120 h, visual observation (*inset*)

Generally, smaller nanoparticles show high activity because of the high surface area to volume ratio. Therefore, 2 mL of the extract was chosen for pH studies.

The pH of the reaction medium is one of the major factors that affects the size and shape of the AgNPs. Here, three different pHs were tested, i.e., pH 5 (acidic region), pH 7 (neutral region) and pH 9 (basic region). The pH was adjusted using dilute H_2SO_4 and NaOH. Figure 4 shows the effects of pH on the synthesis of AgNPs using 2 mL of the *C. officinale* extract at 120 h. The results showed that the SPR peak was shifted from a higher wavelength to a lower wavelength (blue shift) when the pH was changed from the acidic to basic region (pH 5 to pH 7 and pH 9), which suggested that the size of the AgNPs decreased at neutral and basic region compared to the acidic region [28]. Generally, nucleation and growth processes are two major steps involved in colloidal nanoparticle formation. The rate of the nucleation step determines the size, shape and dispersion nature. When increasing the pH, the nucleation step is very fast, which leads to the formation of smaller particles [29].

Based on the UV–Vis spectra, two different AgNPs synthesized using 2 mL of the extract (λ_{max}-440 nm) and synthesized at pH 9 (λ_{max}-420 nm) were chosen for further characterization and application.

FT-IR Spectroscopy

AgNPs have high reactivity and oxidize easily in the air environment. The capping agents are chemical substances that cover the surface area of AgNPs and prevent them from aggregation. The capping mechanism of phyto-constituents on the AgNPs can be understood easily with the help of FT-IR spectroscopy. Figure 5 presents the FT-IR spectra of the dried aqueous extract of *C. officinale* and the

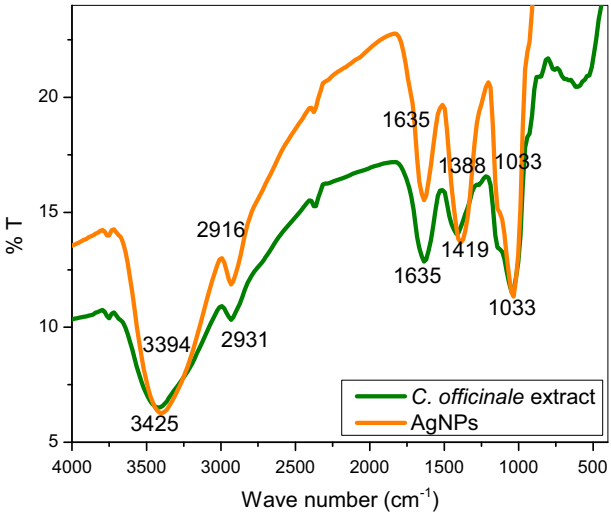

Fig. 5 FT-IR spectra of dried *C. officinale* extract and synthesized AgNPs

synthesized AgNPs. The FT-IR spectra of *C. officinale* showed the major bands at 3425, 2931, 1635, 1419, and 1033 cm^{-1}. The synthesized AgNPs using *C. officinale* showed the absorption bands at 3394, 2916, 1635, 1388, and 1033 cm^{-1}. The bands at 3425 and 3394 cm^{-1} corresponds to the –OH stretching band of the phytoconstituents [30]. The bands at 2931 and 2916 cm^{-1} were attributed to the stretching vibration of the C-H group present in the extract [31]. The bands at 1635 cm^{-1} were assigned to the C=C stretching vibration of the phytoconstituents. The band at 1033 cm^{-1} was assigned to the vibrations of C–O in the constituents. A comparison of both spectra revealed a slight shift in the –OH stretching band in the synthesized AgNPs. The shifting of the band might be due to the involvement of the –OH group present in the phytoextract for capping of the AgNPs [32].

XRD Studies

XRD is a principal characterization tool for obtaining the critical features of metal nanoparticles, such as the crystal structure, crystallite size, particle size, and strain. The AgNPs synthesized using 2 mL extract and AgNPs synthesized at pH 9 were taken for XRD. Figure 6 shows the corresponding XRD patterns. Peak indexing was carried out by comparing the obtained pattern of AgNPs with the standard XRD pattern of crystalline silver. The obtained 2θ values were well correlated with the standard XRD pattern of crystalline silver. The 2θ peaks were indexed to the (111), (200), (220), and (311) planes with face centered cubic geometry [33]. XRD pattern confirmed that both synthesized AgNPs were crystalline with fcc geometrical structure. Using this XRD pattern, the parameters, such as the size of the nanoparticles, d-spacing and lattice constant, were calculated. The calculations were made using Debye–Scherrer Eq. (1) and Bragg's Eq. (2) [34].

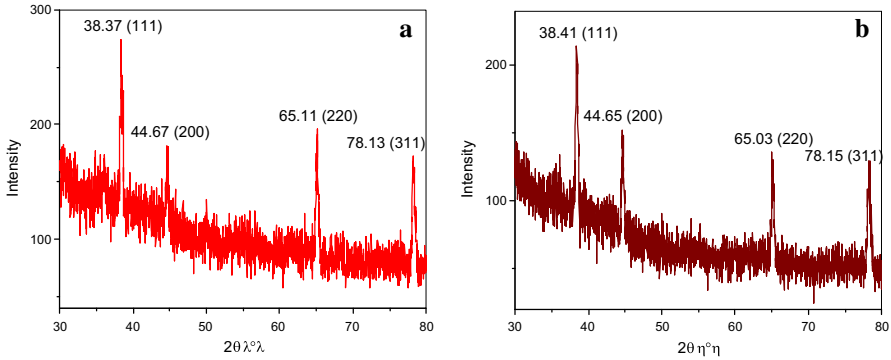

Fig. 6 XRD patterns of AgNPs synthesized using 2 mL extract (**a**) and pH 9 (**b**)

$$L = \frac{k\lambda}{\beta_{1/2}\cos\theta} \tag{1}$$

where L is the average particle size, k is the Gaussian function to fit the peak (0.9), λ is the wavelength of the X-ray (1.54 Å) used for the study, β is the full width half maximum and θ is the angle of reflection.

$$n\lambda = 2d\sin\theta \tag{2}$$

where λ is the wavelength of X-rays (1.54 Å) used for the study, d is the spacing between the planes in the atomic lattice, and θ is the angle between the incident ray and the scattering planes.

Table 1 lists the calculated parameter values. The values were well correlated with the standard values for fcc silver in (JCPDS) file No. 04-0783 [35]. The peak broadening of the XRD pattern (FWHM value) is the key factor in particle size determination. Peak broadening leads to a smaller particle size and vice versa. The calculated values were consistent with the HR-TEM results.

HR-TEM and EDS Analysis

HR-TEM is a direct method to view and analyze the size and shape of nanoparticles, but it is limited to studying only a few particles at a time. The corresponding UV–Vis spectra of the synthesized AgNPs were considered to determine the effects of the SPR shift in UV–Vis spectra on the size of the AgNPs, as shown in Fig. 7. Figures 8 and 9 presents the TEM, SAED pattern, size distribution, and EDS pattern

Table 1 The calculated parameters from the XRD pattern

Sample	Miller indices (hkl)	2θ (°)	FWHM (°)	Average particle size (nm)	d-spacing (Å)	Lattice constant (Å)
AgNPs (2 mL)	(111)	38.37	0.1469	24.06	2.34	4.06
AgNPs (pH 9)	(111)	38.41	0.3628	9.75	2.34	4.05

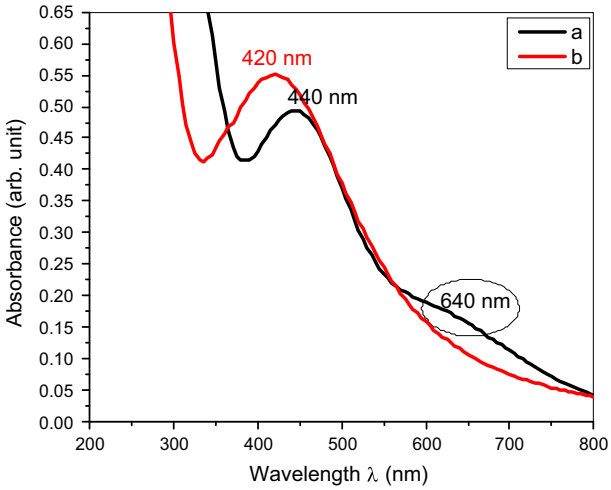

Fig. 7 UV–Vis spectra of synthesized AgNPs using 2 mL extract (**a**) and pH 9 (**b**) taken for HR-TEM analysis

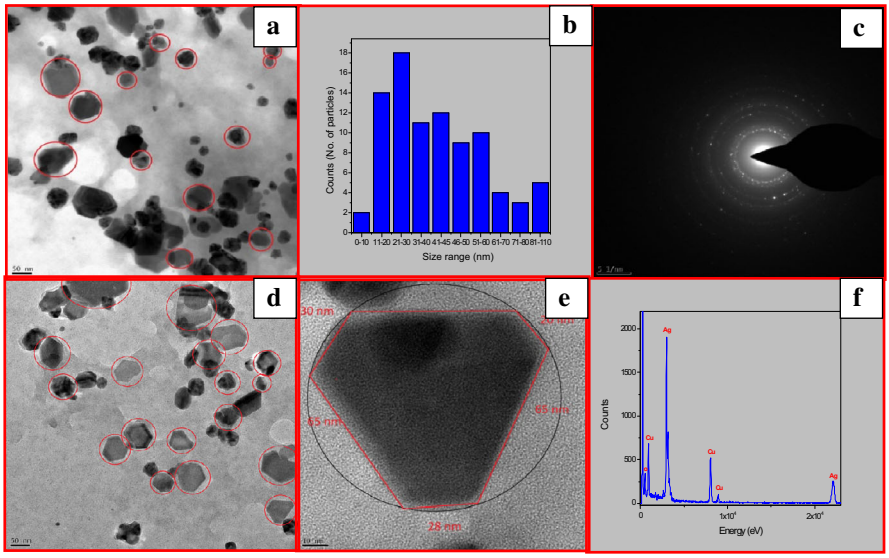

Fig. 8 TEM images of synthesized AgNPs using 2 mL extract at 50 nm scale (**a**), size distribution of AgNPs at 50 nm (**b**), SAED pattern (**c**), at 20 nm scale (**d**), at (10 nm) scale (**e**) and EDS pattern (**f**)

images of AgNPs synthesized using 2 mL of the extract, and AgNPs synthesized at pH 9. Two different sizes and shapes were observed, ~35 nm (truncated triangular prism shape) and ~9 nm (spherical shape). The shape difference in the AgNPs synthesized using 2 mL of the extract is reflected in the absorption of AgNPs; it absorbs two different wavelengths, 440 and 640 nm (truncated triangular prism

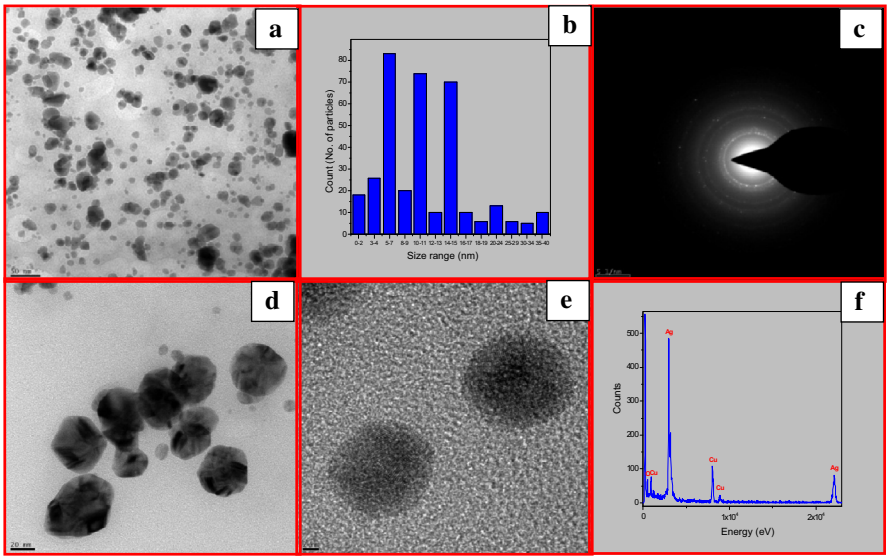

Fig. 9 TEM images of synthesized AgNPs at pH 9 at 50 nm scale (**a**), size distribution of AgNPs at 50 nm (**b**), SAED pattern (**c**), at 20 nm scale (**d**), at 10 nm scale (**e**) and EDS pattern (**f**)

shape) [36, 37]. The SAED pattern of both AgNPs revealed diffraction rings with white dots representing the (111), (200), (220), and (311) planes of fcc AgNPs. The EDS profile confirmed that the synthesized AgNPs were well distributed on the carbon coated copper disc. The other peaks were attributed to the presence of copper metal.

Figure 10 shows the high resolution images of single AgNPs synthesized using 2 mL extract and pH 9. The crystalline lattice fringes were observed clearly. The d-spacing (the distance between two parallel lattice fringes) were calculated to be 0.24 nm, which corresponds to the (111) plane of fcc geometry of crystalline Ag. The calculated results were consistent with the XRD patterns as well as with previous reports [38].

Catalytic Activity of AgNPs

The catalytic activities of the two different morphological AgNPs on the reduction of 4-nitroaniline using $NaBH_4$ as a reducing agent were investigated. 4-NA in water absorbs in the visible region at 380 nm. The reduction reaction of 4-NA can be monitored easily by UV–Vis spectroscopy by measuring the decrease in the absorbance intensity at 380 nm. The reduction reaction of 4-NA by $NaBH_4$ did not take place in the absence of the AgNPs [39]. After adding the AgNPs, immediate reduction takes place, which was observed visually from the gradual disappearance of the yellow color. The reduction reaction was monitored every 30 s using UV–Vis spectrophotometer. Figures 11 and 12 presents the UV–Vis spectra of the catalytic reduction of 4-NA by the truncated triangular AgNPs (~35 nm) and spherical

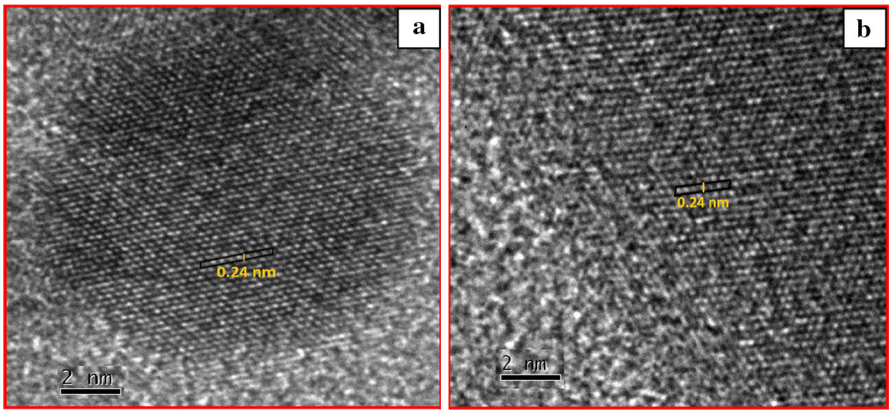

Fig. 10 HR-TEM images of synthesized AgNPs at pH 9 (**a**) and using 2 mL extract (**b**)

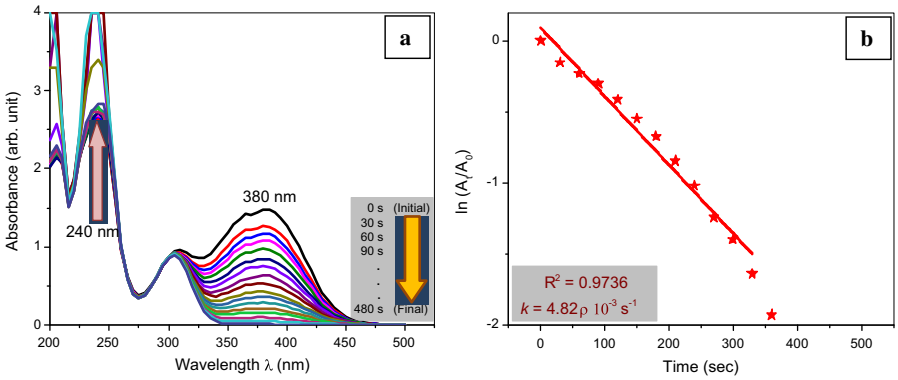

Fig. 11 UV–Vis spectra of catalytic reduction of 4-NA by truncated triangular shaped AgNPs (~35 nm) (**a**) and ln (A_t/A_0) versus time plot for that reduction (**b**)

AgNPs (~9 nm) with its ln (A_t/A_0) vs. time graphs. The reduction of 4-NA by $NaBH_4$ in the presence of AgNPs followed pseudo first order reaction kinetics. The linear relationship between ln (A_t/A_0) and time were noticed from the value of R^2 (linearity factor). The rate constant (k) of the reaction with the truncated triangular AgNPs and spherical AgNPs were calculated from the slope of the straight line to be 4.82×10^{-3} s^{-1} and 11.16×10^{-3} s^{-1}, respectively. From the results, the reduction of 4-NA catalyzed by spherical AgNPs was much faster than the truncated triangular AgNPs. The change in catalytic activity can be explained in terms of the size effect.

Figure 13 presents a plausible mechanism for the catalytic reduction of 4-NA. In this catalytic reduction, $NaBH_4$ acts as electron donor and hydrogen supplier, the AgNPs are an electron transfer mediator that collects electron from BH_4^- ion to 4-NA [40, 41]. The simultaneous adsorption of hydrogen species from BH_4^- and

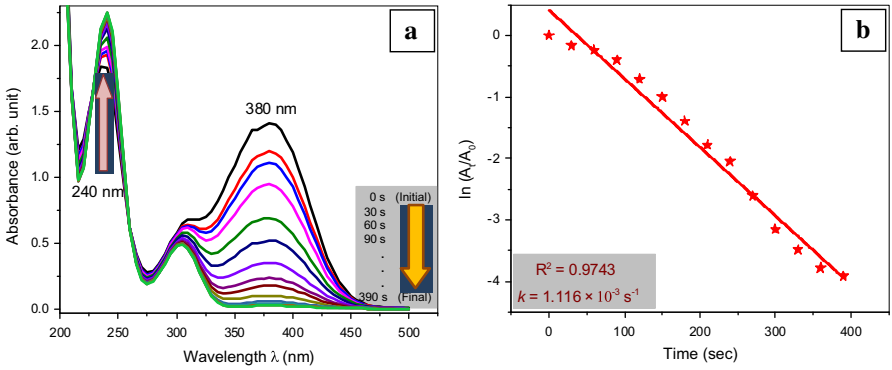

Fig. 12 UV–Vis spectra of catalytic reduction of 4-NA by spherical AgNPs (~9 nm) (**a**) and ln (A_t/A_0) versus time plot for that reduction (**b**)

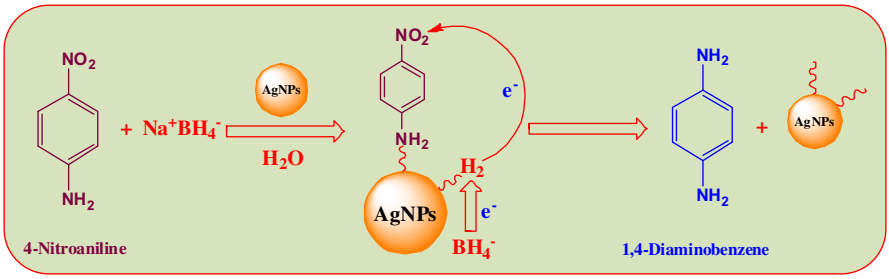

Fig. 13 Plausible mechanism for the catalytic reduction of 4-NA by $NaBH_4$ using AgNPs as a catalyst

4-NA on the surface of AgNPs takes place and diffusion between the adsorbed species leads to desorption of the product [42]. In addition, the AgNPs relay electrons to catalyze the reduction. The small sized spherical nanoparticles have a large surface area to volume ratio, which can offer more catalytic sites than the larger sized nanoparticles. Moreover, the larger AgNPs have more steric interactions between the adsorbed species compared to the smaller AgNPs. These steric interactions may decrease the adsorption rate of the reactants [43]. Therefore, the rate of catalytic reduction was higher on the ~9 nm spherical shaped AgNPs than ~35 nm truncated triangular AgNPs. The final product, 1,4-Diaminobenzene was confirmed by comparing the TLC of synthesized product with that of commercial sample.

Conclusion

The AgNPs were synthesized with two different morphologies using an aqueous extract of *Cnidium officinale* as a green reducing and capping source. The synthesized AgNPs were prevented from aggregation by the phyoconstituents

present in the extract, as determined by FT-IR spectroscopy. XRD and HR-TEM showed that the synthesized AgNPs were crystalline with fcc geometry and the results were consistent with the standard data. The mean size of the AgNPs synthesized using 2 mL extract and AgNPs synthesized at pH 9 are $\sim$35 and $\sim$9 nm, respectively. The size dependent catalytic activities of the AgNPs were observed in the reduction of 4-NA in water by $NaBH_4$ (reducing agent) as a test reaction. The AgNPs with a $\sim$9 nm size showed superior catalytic activity than $\sim$35 nm sized AgNPs. The calculated rate constant (k) for the reduction of 4-NA by the spherical $\sim$9 nm sized AgNPs was 11.16×10^{-3} s^{-1}.

Acknowledgments This study was supported by Priority Research Centers Program through the National Research Foundation of Korea (NRF) funded by the Ministry of Education (2014R1A6A1031189).

References

1. J. L. Elechiguerra, J. Reyes-Gasga, and M. J. Yacaman (2006). *J. Mater. Chem.* **16**, 3906.
2. K. L. Kelly, E. Coronado, L. L. Zhao, and G. C. Schatz (2003). *J. Phys. Chem. B* **107**, 668.
3. M. Chen, Y. Cai, Z. Yan, and D. W. Goodman (2006). *J. Am. Chem. Soc.* **128**, 6341.
4. C. Medina, M. J. Santos-Martinez, A. Radomski, O. I. Corrigan, and M. W. Radomski (2007). *Br. J. Pharmacol.* **150**, 552.
5. A. Moores and F. Goettmann (2006). *New J. Chem.* **30**, 1121.
6. T. K. Sau, A. L. Rogach, F. Jackel, T. A. Klar, and J. Feldmann (2010). *Adv. Mater.* **22**, 1805.
7. K. G. Stamplecoskie and J. C. Scaiano (2010). *J. Am. Chem. Soc.* **132**, 1825.
8. Z. Sadowski, I. H. Maliszewska, B. Grochowalska, I. Polowczyk, and T. Kozlecki (2008). *Mater. Sci-Poland* **26**, 419.
9. S. Yallappa and J. Manjanna (2014). *J. Clust. Sci* **25**, 1449.
10. S. J. Hoseini, M. Darroudi, R. K. Oskuee, L. Gholami, and A. K. Zak (2015). *Adv. Powder Technol* **26**, 991.
11. A. Miri, M. Sarani, M. R. Bazaz, and M. Darroudi (2015). *Spectrochim. Acta A* **141**, 287.
12. M. Venkatesham, D. Ayodhya, A. Madhusudhan, A. S. Kumari, G. Veerabhadram, and K. G. Mangatayaru (2014). *J. Clust. Sci.* **25**, 409.
13. S. Iravani (2011). *Green Chem.* **13**, 2638.
14. S. A. Umoren, I. B. Obot, and Z. M. Gasem (2014). *J. Mater. Environ. Sci.* **5**, 907.
15. M. Noruzi, D. Zare, and D. Davoodi (2012). *Spectrochim. Acta A* **94**, 84.
16. J. B. Jeong, J. H. Park, H. K. Lee, S. Y. Ju, S. C. Hong, J. R. Lee, G. Y. Chung, J. H. Lim, and H. J. Jeong (2009). *Food Chem. Toxicol.* **47**, 525.
17. M. Ramalingam and P. Yong-Ki (2010). *Pharmacogn. Mag.* **6**, 323.
18. K. Bae, Y. Choi, S. Kim, and Y. Kim (2011). *Molecules* **16**, 8833.
19. T. Tsukamoto, Y. Ishikawa, and M. Miyazawa (2005). *J. Agric. Food Chem.* **53**, 5549.
20. J. Kwon and Y. Ahn (2002). *J. Agric. Food Chem.* **50**, 4479.
21. R. V. Jagadeesh, G. Wienhofer, F. A. Westerhaus, A. Surkus, M. Pohl, H. Junge, K. Junge, and M. Beller (2011). *Chem. Commun.* **47**, 10972.
22. K. Li, Z. Zheng, J. Feng, J. Zhang, X. Luo, G. Zhao, and X. Huang (2009). *J. Hazard. Mater.* **166**, 1180.
23. S. Eustis and M. A. El-Sayed (2006). *Chem. Soc. Rev.* **35**, 209.
24. M. Umadevi, M. R. Bindhu, and V. Sathe (2013). *J. Mater. Sci. Technol.* **29**, 317.
25. T. J. I. Edison and M. G. Sethuraman (2013). *Spectrochim. Acta A* **104**, 262.
26. A. Parveen and S. Rao (2015). *J. Clust. Sci.* **26**, 1295.
27. S. L. Smitha, K. M. Nissamudeen, D. Philip, and K. G. Gopchandran (2008). *Spectrochim. Acta A* **71**, 186.
28. T. J. I. Edison and M. G. Sethuraman (2012). *Process Biochem.* **47**, 1351.
29. S. K. Mehta, S. Chaudhary, and M. Gradzielski (2010). *J. Colloid Interface Sci.* **343**, 447.
30. A. J. Kora, S. R. Beedu, and A. Jayaraman (2012). *Org. Med. Chem. Lett.* **2**, 1.

31. N. Basavegowda, K. B. S. Magar, K. Mishra, and Y. R. Lee (2014). *New J. Chem.* **38**, 5415.
32. S. Sing, P. Patel, S. Jaiswal, A. A. Prabhune, C. V. Ramana, and B. L. V. Prasad (2009). *New J. Chem.* **33**, 646.
33. N. Singh and P. K. Khanna (2007). *Mater. Chem. Phys.* **104**, 367.
34. S. Li, Y. Shen, A. Xie, X. Yu, L. Qiu, L. Zhang, and Q. Zhang (2007). *Green Chem.* **9**, 852.
35. S. Sadhasivam, P. Shanmugam, and K. Yun (2010). *Colloids Surf. B* **81**, 358.
36. I. A. Wani, A. Ganguly, J. Ahmed, and T. Ahmad (2011). *Mater. Lett.* **65**, 520.
37. B. Tang, L. Sun, J. Li, M. Zhang, and X. Wang (2015). *Chem. Eng. J.* **260**, 99.
38. T. Tan, C. Tian, Z. Ren, J. Yang, Y. Chen, L. Sun, Z. Li, A. Wu, J. Yin, and H. Fu (2013). *Phys. Chem. Chem. Phys.* **15**, 21034.
39. S. Kundu, K. Wang, and H. Liang (2009). *J. Phys. Chem. C* **113**, 5157.
40. A. Gangula, R. Podila, M. Ramakrishna, L. Karanam, C. Janardhana, and A. M. Rao (2011). *Langmuir* **27**, 15268.
41. A. Hernández-Gordillo and V. R. González (2015). *Chem. Eng. J.* **261**, 53.
42. S. Wunder, F. Polzer, Y. Lu, Y. Mei, and M. Ballauff (2010). *J. Phys. Chem. C* **114**, 8814.
43. V. Reddy, R. S. Torati, S. Oh, and C. Kim (2013). *Ind. Eng. Chem. Res.* **52**, 556.